BALKAN JOURNAL OF ELECTRICAL & COMPUTER ENGINEERING, Vol. 13, No. 3, September 2025
Research Article

Calculation of Power Losses for SiC MOSFET Based 3-Phase 3-Level T-Type Inverter

Erkan Deniz and Berkan Turan

***Abstract*— In recent years, interest in highly efficient and compact power converters in power electronics applications has been increasing day by day. In this study, a SiC MOSFET-based 3-level (3L) T-Type inverter (TNPC) is proposed to obtain a high-efficiency and compact converter. Considering the MSCSM120HRM163AG-SiC-MOSFET intelligent power modules (IPM) developed by Microchip for 3L T-Type inverter, the power losses of a 3-phase 3-level T-Type inverter are calculated in MATLAB environment. To demonstrate the efficiency of SiC MOSFET based T-Type Inverter, a 3-phase 3L T-Type inverter feeding a vector-controlled 3-phase PMSM is simulated using MATLAB/Simulink and Simscape blocks. In the simulation, the PMSM is operated at different speed references under almost full load (42.09 Nm). While the PMSM operates at 3000 rpm under 40Nm load, the voltage-current waveforms of the SiC MOSFETs in the T-Type inverter are obtained. Using these waveforms and the data from the data sheets of the IPMs, the power losses of the 3L TNPC inverter are calculated for different switching frequencies. The Space Vector PWM method used to generate 50 kHz PWM signals for the 3L T-Type inverter also ensures that the dc-link capacitor voltages remain balanced. In addition, the variations of line-to-line voltage and dc-link capacitor voltages of the inverter and the variations of speed, torque, rotor position, d-q currents, and stator currents of the PMSM are given.**

Index Terms—**Three-level T-Type inverter, SiC MOSFET, power loss calculation, PMSM, space vector PWM (SVPWM).**

I. Introduction

FOR NEARLY a quarter century, Si-based multilevel PWM converters have been used in many applications, including motor drives, energy storage systems, static VAr compensation, HVDC, renewable energy systems, battery chargers in electric vehicles, microgrids, etc. Because, they have advantageous features such as being suitable for the use of lower-voltage rating switches, low dv/dt ratio that results from the reduced voltage stress, low common mode voltage, output voltage-current waveforms with lower THD, and smaller output filter size [1,2]. The low dv/dt minimizes Electromagnetic Interference (EMI) issues. However, increasing the number of levels in MLIs leads to an increase in the number of switches, which increases the design and control complexity and power losses of the converter [3]. Therefore, there is a growing interest in 3-level (3L) converters in low and medium voltage power electronics applications because 3L topologies require less devices and gate drivers that do not cause control complexity and large size. Multilevel converters come in three conventional topologies: cascade, capacitor-clamped, and diode-clamped. With this, as it eliminates the need for multiple isolated dc-link sources and large clamping capacitors, the 3L diode-clamped topology is widely preferred in industrial applications. There are three widely recognized types of diode clamping converters: conventional neutral point clamped (NPC) [4], active NPC (ANPC), and T-Type. While ANPC is proposed in [5] to solve the problem of unbalanced power losses between semiconductors in the NPC circuit, T-Type converter is proposed as a result of studies carried out to reduce the number of semiconductors in the NPC circuit in [6]. 3L T-type topology provides maximum efficiency and lower cost compared to other topologies such as 3L NPC, 3L ANPC, and 3L flying capacitor due to its simple operating principle, less power devices and isolated gate driver requirements, lower power losses, and smaller converter size [7-9]. Nevertheless, the semiconductors (S_1, S_4) in the legs connected to the +dc and -dc busbars of the 3L T-type converter must have higher-rated voltages than those in the other 3L topologies [10]. The efficiency of 3L NPC and T-type inverters is evaluated for switched reluctance motor drives in hybrid electric vehicles and it was shown that the T-type inverter provides superior energy savings [11]. In [12], the power loss comparison of Si IGBT-based 3L NPC and T-type inverters is investigated for different modulation techniques. Since there are not two series-connected switches in the inverter leg, the power losses of the T-type are lower than those of the NPC. Low power losses extend the life of the converter and reduce the size of the heat sinks. Moreover, smaller and less expensive filters can be employed to filter EMI noise since the T-type inverter permits reduced EMI emissions [13]. However, 3L-TNPC suffers from high power loop leakage inductance due to the complex power loop structure like other three-level topologies. To reduce the leakage inductances, a SiC-MOSFET based 3L-TNPC power modules are usually preferred. In [14], a SiC-MOSFET-based 3L-TNPC power module with hybrid packaging method is proposed.

The more compact and highly efficient power electronic converters, which are the basic building blocks of electrical energy conversion applications, are designed, the more certain it is that the size of the entire system will be significantly reduced and its efficiency increased [15]. Using wide bandgap

Erkan Deniz, is with Department of Electrical Electronics Engineering Firat University, Elazığ, Turkey,(e-mail: ededeniz@firat.edu.tr).
https://orcid.org//0000-0002-9048-6547

Berkan Turan, is with TCDD-Republic of Turkey State Railways, Elazığ, Turkey, (e-mail: turanberkan23@gmail.com).
https://orcid.org/0000-0003-4304-0099

Manuscript received Jan 14, 2025; accepted Feb 9, 2025.
DOI: 10.17694/bajece.1619631

(WBG) SiC MOSFETs for the 3L T-Type inverter can enable the creation of a compact and highly efficient power converter. Because, SiC MOSFETs offer higher breakdown voltages, higher switching frequencies, lower switching losses, higher operating temperatures, low turn-on resistances, low stray inductance, and smaller chip size compared to Si-based semiconductors, which allows for increased power density and reduced size of passive components in converters [16-18]. Using gate drivers with features such as “noise robustness, fast response protection, and accurate slew-rate control” will enable full utilization of SiC MOSFETs. Nevertheless, it raises concerns regarding electromagnetic compatibility (EMC) since high switching frequencies generate more overshoot, causing EMI noises, and making interference optimization difficult in printed circuit board (PCB) layout and EMI filter design [19,20]. Therefore, all power converters using high switching frequencies require the use of EMI filters. However, EMI filter design is a very complex and specialized subject of study and expertise depending on the converter type and PCB layout.

EMI, which emerges in power converters in two forms, such as *Conducted* through power traces and *Radiated* through electromagnetic fields, can hamper the proper operation of both the converter itself and nearby electronic devices. The process of designing filters for the suppression of EMI noises starts with the identification of EMI sources caused by high-frequency switching, fast current (di/dt) and voltage (dv/dt) changes in the converter power circuit. EMI sources vary for different PCB layouts and different PWM methods, even for the same converter. For this purpose, all parasitic capacities between SiC-MOSFETs and +dc, -dc, neutral busbars, and heat sinks are calculated using the designed PCB layout [21]. In the next step, based on an applicable regulatory standard such as IEC, CISPR, FCC, maximum admissible EMI levels at various frequencies should be determined, and frequency ranges around the switching harmonics where noise is most prominent should be defined. For example, according to standards such as CISPR 16-1-2 and IEC 61000-6-3, the frequency range in which the electromagnetic noise of a device radiated over electrical lines must be limited is 150 kHz to 30 MHz [22].In the last stage, common mode and differential mode filters are usually preferred and designed. Inductors in these filters are selected according to their impedance characteristics at noise frequencies, while capacitors are selected for their high-frequency filtering properties. Simulation tools are used to verify the performance of the filter, followed by prototype development and EMI testing to verify its effectiveness [23].

In this work, a SiC-MOSFET based 3L T-Type topology is proposed to obtain a highly efficient and compact dc/ac converter for low-voltage (<1kV) power electronics applications. The switching frequency is chosen as 50kHz to reduce the size of the passive components and switching losses in the converter circuit. In order to demonstrate the high efficiency operation of the inverter circuit, a 3L T-type inverter driving a 3-phase PMSM is simulated in MATLAB. In order to reduce EMI issues while utilizing the high switching frequency, Microchip MSCSM120HRM163AG-SiC-MOSFET intelligent power modules (IPMs) are considered for the phase legs of the 3L T-Type inverter. The conduction and switching losses of the 3L TNPC are calculated by taking into account the current-voltage waveforms of the SiC-MOSFETs and the information on the data sheets of the SiC-MOSFETs in the most demanding operating condition of the inverter. For a more accurate calculation, the average and effective values of the currents flowing through the SiC-MOSFETs and body diodes are also measured for each half of the switching period. Similar measurements are made for the voltages at the terminals of the SiC-MOSFETs and gap diodes.

II. Operation of 3-Level T-Type Inverter Topology

In high-power applications and especially at high switching frequencies, the large number of power devices on PCBs increases EMI noises. This causes overshoots and ringing in the converter output voltage. For this reason, as a result of studies carried out to reduce the number of semiconductors for 3-level converters, the first T-Type inverter was proposed in [6]. A 3L T-Type inverter, also known as a Neutral Point Piloted (NPP) inverter, consists of a split dc-link and twelve MOSFETs with body diodes, as seen in Figure 1. There are two series switches on each phase leg as in a two-level inverter, and the middle point of one leg is connected to the middle of the dc-link via a bidirectional power device. In Fig.1, S_{1X} and S_{4X} have twice the rated voltage of switches S_{2X} and S_{3X} connected to the neutral point [24].

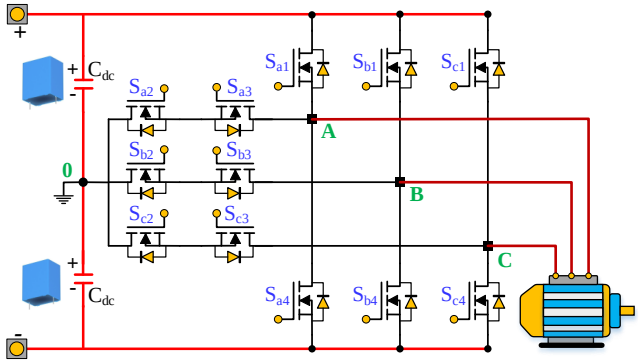

Fig.1. Circuit of 3-phase 3L T-Type inverter

TABLE I
SWITCHING STATES OF A 3L T-TYPE INVERTER

		Power Devices				V_{out}
		S_{1X}	S_{2X}	S_{3X}	S_{4X}	V_{A0}
Switching States	P	1	1	0	0	$+V_{dc}/2$
	O	0	1	1	0	0
	N	0	0	1	1	$-V_{dc}/2$

The switching states of the 3L T-Type inverter and the corresponding output phase-neutral voltage values are given in Table I. The output of a phase leg is connected via S_{1X} and S_{4X} to the dc-link's positive (P) and negative (N) voltage levels, and via S_{2X}-S_{3X} to the zero (O) level [25]. As seen in Table I, inverter phase-neutral voltage is obtained in 3-levels as $-V_{dc}/2$, 0 and $+V_{dc}/2$ for the three possible switching states shown as N, O, and P. The output phase-phase voltage of the inverter has five levels at $-V_{dc}$, $-V_{dc}/2$, 0, $+V_{dc}/2$, and $+V_{dc}$ values. The positive and negative current pathways during the change from the P to the O switching state are shown in Fig.2 [24].

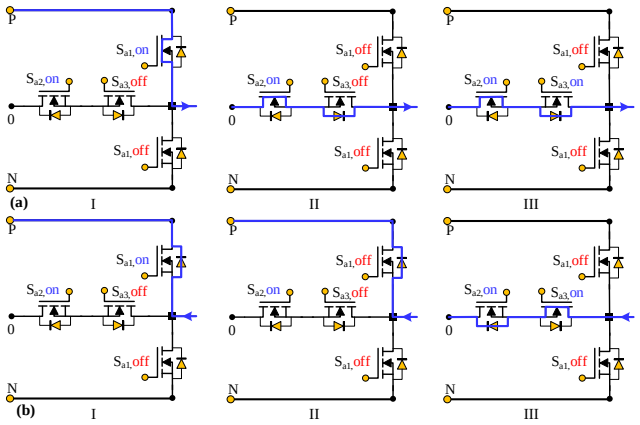

Fig.2. Current commutation during transition from switching state P to 0 (a) positive I_{out} , (b) negative I_{out}

III. SVPWM TECHNIQUE FOR 3L T-TYPE INVERTER

The Space Vector PWM (SVPWM) technique for a voltage source inverter is based on representing the ac desired output voltages from the inverter with a reference voltage space vector in α-β space. The instantaneous values of desired ac output voltages can be used to determine the $\vec{V}_{ref}$ vector's amplitude and phase angle. If the voltages are sinusoidal and balanced, the vector will rotate at a constant angular velocity and will have a constant amplitude [26, 27]. Considering the 3-phase legs of the inverter, the 3L T-Type inverter has 27 switching states, and each of these switching states can be represented as a vector using Eq.(1). As a result, a total of 27 voltage vectors are formed, as seen in Table II. Figure 3 shows the space-vector diagram of the 3L T-Type inverter, which is created when all voltage vectors are positioned in the α-β plane [28]. As seen in Figure 3, while the voltage vectors are constant, the reference voltage vector rotates with an angular speed ω. The space-vector diagram has six sectors, each of which is separated into four regions, as shown in Fig.3.

TABLE II
VOLTAGE VECTORS CORRESPONDING TO SWITCHING STATES

Type	Vectors						Length
Zero	PPP	OOO	NNN				**0**
Small	POO	PPO	OPO	OPP	OOP	POP	$V_{dc}/3$
	ONN	OON	NON	NOO	NNO	ONO	
Medium	PON	OPN	NPO	NOP	ONP	PNO	$V_{dc}/\sqrt{3}$
Large	PNN	PPN	NPN	NPP	NNP	PNP	$2V_{dc}/3$

$$\vec{V} = \frac{2}{3}\left(V_a\, e^{j0} + V_b\, e^{j2\pi/3} + V_c\, e^{-j2\pi/3}\right) \qquad (1)$$

The calculation of voltage vectors' dwell times for a 3L T-Type inverter is based on the principle of "*Volt-Second Balancing*" principle [29]. Therefore, the reference vector is formed by the three closest vectors. For example, when the reference vector $\vec{V}_{ref}$ is located in region-2 of Sector-1, the three closest vectors are $\vec{V}_1$, $\vec{V}_2$, and $\vec{V}_7$. In this case, voltage-time equalization is as shown in Eq.(2).

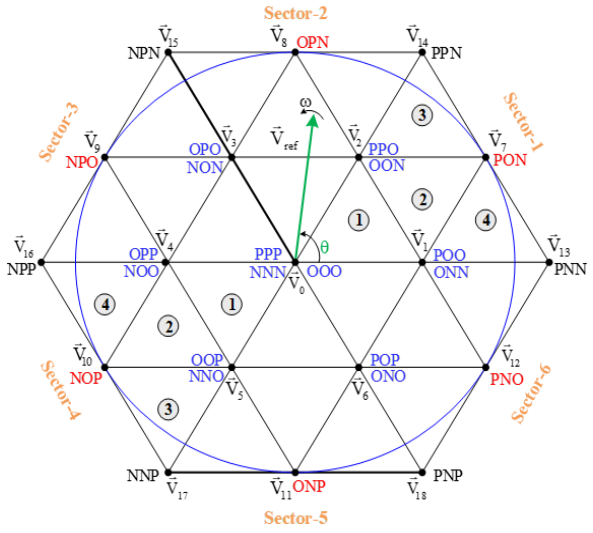

Fig.3. Space-vector diagram for 3L T-Type inverter

$$\begin{aligned} \vec{V}_1.T_a + \vec{V}_7.T_b + \vec{V}_2.T_c &= \vec{V}_{ref}.T_s \\ T_a + T_b + T_c &= T_s \end{aligned} \qquad (2)$$

Here, T_a, T_b, and T_c are the dwell times of $\vec{V}_2$, $\vec{V}_7$ and $\vec{V}_{14}$, respectively. By writing voltage-second balancing equations for other regions in Sector-1 and substituting vector values in these equations, dwell times for all regions can be found as given in [28]. After calculating the dwell times for each sector and region, PWM signals should be generated by determining the application order of space vectors according to the sector and region where $\vec{V}_{ref}$ is located. In this study, the order of application of vectors for minimum THD is determined [29]. For region-3 and region-4 in Sector-2, the application order of space vectors and accordingly the switching schemas of phases a, b, and c of the T-Type inverter are given in Fig.4.

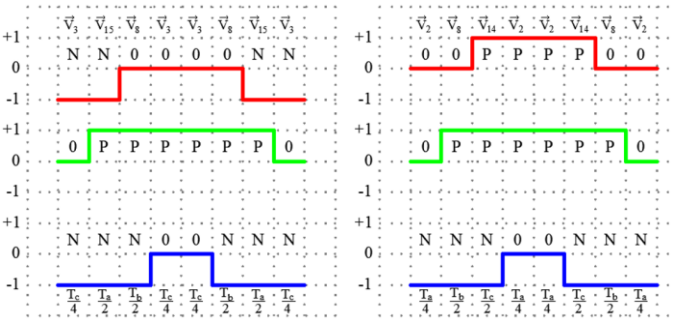

Fig.4. Switching states of inverter phase legs (a) region-3, (b) region-4

IV. FIELD ORIENTED CONTROL FOR 3-PHASE PMSM

When forming the dynamic mathematical model of a PMSM, the components of the machine can be expressed in three different reference frameworks such as stator reference frame (3-phase model), fixed 2-phase reference frame (2-phase α-β model), and rotor reference frame (2-phase d-q model) [30, 31]. Since stator winding inductances vary depending on the rotor

position, the rotor-referenced d-q model is preferred in this study. In this model, the stator currents are converted into virtual two-phase d-q axis currents that rotate with the electrical speed of the rotor. Thus, inductance values that do not change depending on the position of the rotor are obtained for the counterpart of the stator windings on the d-q axis set. Since the rotor speed is equal to the synchronous speed, this model is also called the d-q model with synchronous reference [32, 33]. The Kirchhoff voltage law can be used to derive the PMSM equations, which are provided in Eq. (3) and (4).

$$u_d = R_s\, i_d + \frac{d}{dt}\psi_d - \omega_r\, \psi_q \tag{3}$$

$$u_q = R_s\, i_q + \frac{d}{dt}\psi_q - \omega_r\, \psi_d \tag{4}$$

Where ω_r is the electrical rotor frequency and R_s is the stator winding resistance. The linkage fluxes of the d- and q-axes, $\vec{\psi}_d$ and $\vec{\psi}_q$, are given in Eqs. (5) and (6).

$$\psi_d = \psi_m + L_d i_d \tag{5}$$

$$\psi_q = L_q i_q \tag{6}$$

Where ψ_m is the flux linkage due to the rotor magnets and its derivative is zero since it is a constant value. The electromagnetic torque for a PMSM is expressed in terms of the d and q-axis components as follows:

$$T_e = \frac{3}{2} P(\psi_d i_q - \psi_q i_d) \tag{7}$$

Where P is the pole pair number. To achieve a basic control similar like a dc motor, I_q and I_d are controlled by a vector control algorithm.

Field Oriented Control (FOC) is the most widely known vector control technique. The basic principle of FOC is the separation of 3-phase stator currents into two separate d-q components that produce torque and flux. Thus, magnetic flux and torque control are controlled independently of each other. Torque and flux are controlled by the stator current components in the rotor reference plane, I_d and I_q, respectively. However, the effectiveness of the I_d component in control is eliminated because permanent magnets supply the flux in PMSMs. Therefore, controlling just I_q will be sufficient in moment control. To obtain the components of the stator currents in the rotor reference plane (I_d-I_q) in FOC, position information about the rotor is required. The block diagram of the FOC for a PMSM is given in Figure 5 [23, 31]. As seen in Fig.5, the speed of the motor is measured with an encoder and compared with the reference speed. The error is applied to a PI speed controller and the reference I_{q_ref} is obtained from the controller output. Since the flux for the motor is provided by permanent magnets, the reference value I_{d_ref} is taken as zero. Besides, after the 3-phase stator currents (I_{abc}) of the motor are measured with sensors, d-q current components (I_d-I_q) are obtained using the Park Transformation. These current components are compared with the reference current components (I_{d_ref}, I_{q_ref}), and the current errors are applied to PI controllers. At the output of the PI controllers, the components of the reference voltages (V_{d_ref}, V_{q_ref}) that the T-Type inverter is required to produce are obtained. These reference voltages are then converted into 3-phase reference voltages for the three-level SVPWM algorithm using the Inverse Park Transform. As a result, the 3L T-Type inverter is switched with SVPWM signals, and the voltages required by the PMSM for different speed references and load cases are generated.

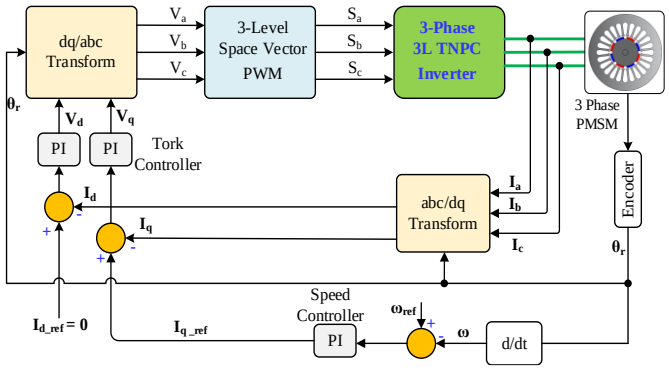

Fig.5. The block diagram of the FOC for a PMSM

V. MATLAB SIMULATION OF 3L T-TYPE INVERTER SUPPLYING 3-PHASE PMSM

In this study, the field-oriented vector control of a 3-phase PMSM fed by a 3L T-Type inverter is simulated by using MATLAB/*Simulink* and *Simscape Electrical* blocks. The general view of simulation is given in Figure 6. The eighteen SiC MOSFETs are used to create a 3-phase 3L T-Type inverter, which is switched by 50kHz 3-level SVPWM signals. In simulation, a PMSM with 8 poles, 3000 rpm, and 42.09 Nm nominal values is preferred as a motor. Other parameters of the PMSM are given in *Appendix-A*.

In the simulation, the variations of the motor speed, torque, rotor position, stator currents, inverter line-to-line voltage, and inverter dc-link capacitor voltages are analyzed for different reference speeds. The motor is continuously loaded with a constant load of 40 Nm. As seen in Figure 7, the motor reaches the reference speed given as 1500 rpm at t=0 in approximately 0.1s. The PMSM smoothly follows this reference speed which is kept constant until t=1.0s. Then the reference speed is changed to 3000 rpm at t=1.0s and -3000 rpm at t=2.0s. The vector control enabled the engine to reach these reference speeds in a very short time and to follow the reference speed stably. The change of moment produced by PMSM is given in Figure 8.As seen in Figure 8, it is seen that the PMSM produces high moments in transients, while it produces a constant moment of approximately 40 Nm in steady states. Also, at the reference speed change of -3000 rpm at t=2.0s, the PMSM produces a negative moment.

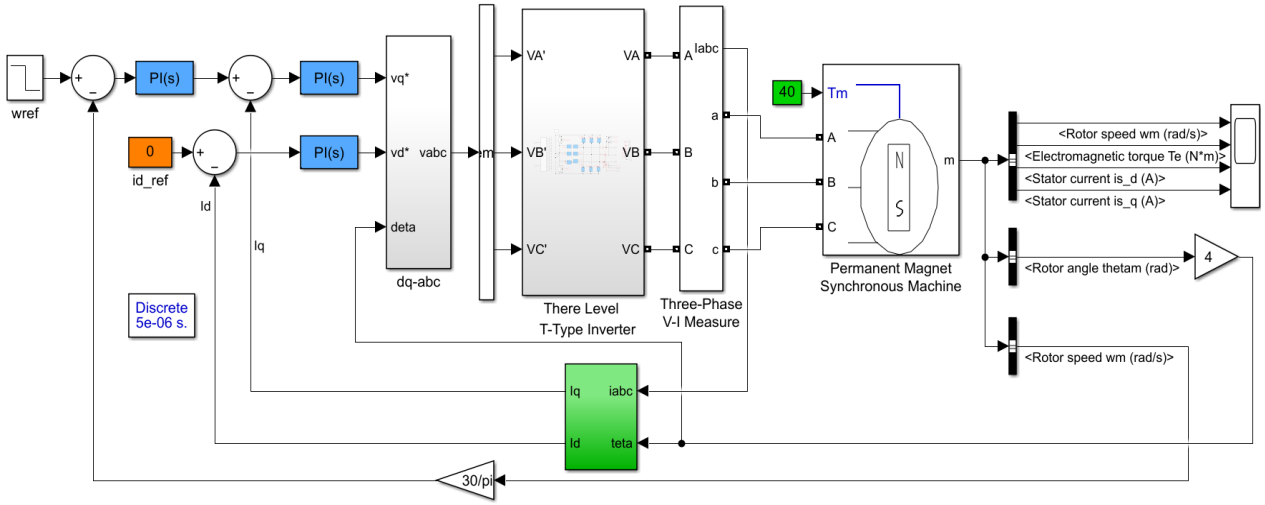

Fig.6. MATLAB simulation of PMSM fed by 3L T-Type inverter

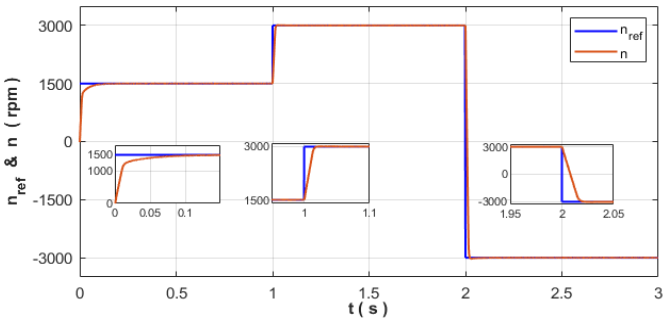

Fig.7. The speed of PMSM for Te= 40N.m and n_{ref} = 1500rpm, ±3000rpm

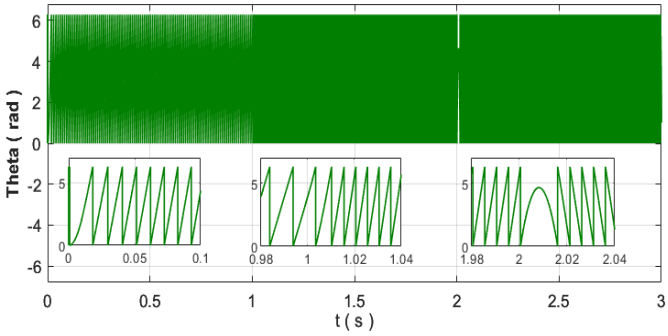

Fig.9. The rotor's position angle for T_e= 40N.m and n_{ref} = 1500rpm, ±3000rpm

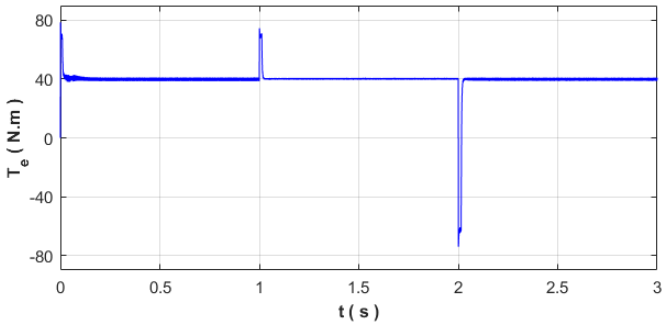

Fig.8. Tork of PMSM for T_e= 40N.m and n_{ref} = 1500rpm, ±3000rpm

The rotor's electrical position angle (Theta) is given in Figure 9. As seen from the figure, the theta passes through the zero point every 2π radians. In the reference speed changes at t=0, 1.0s and 2.0s, the FOC changed the rotor's position angle appropriately and quickly, as seen in Figure 9. The rotor's electrical angle has a frequency of 100Hz for 1500 rpm and 200 Hz for ±3000 rpm.

For reference speeds of 1500 rpm, and ±3000 rpm under T_e=40 Nm load, the waveforms of the flux component I_d and moment component I_q of the current are given in Figure 10 and the 3-phase stator currents with THD analysis are given in Figure 11. As can be seen from the figures, both stator currents and I_q current reached high values during the transient times. However, in steady states, both remain constant at their nominal values. Besides, as expected, the value of the I_d component is not affected by the speed changes and remains at zero all the time. The total harmonic distortion of stator currents is obtained as 1.67% for 1500 rpm speed reference at t=0.5s and 1.36% for +3000 rpm reference speed at t=1.5s.

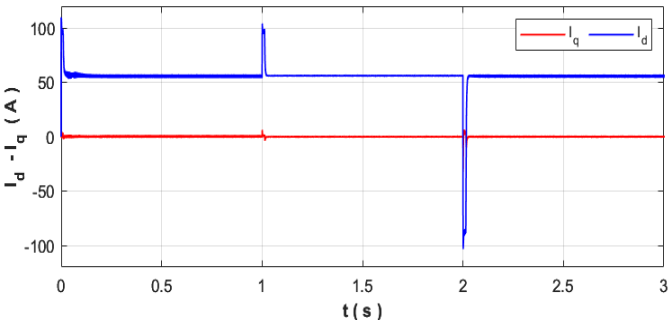

Fig.10. The I_d-I_q components for T_e= 40N.m and n_{ref} = 1500rpm, ±3000rpm

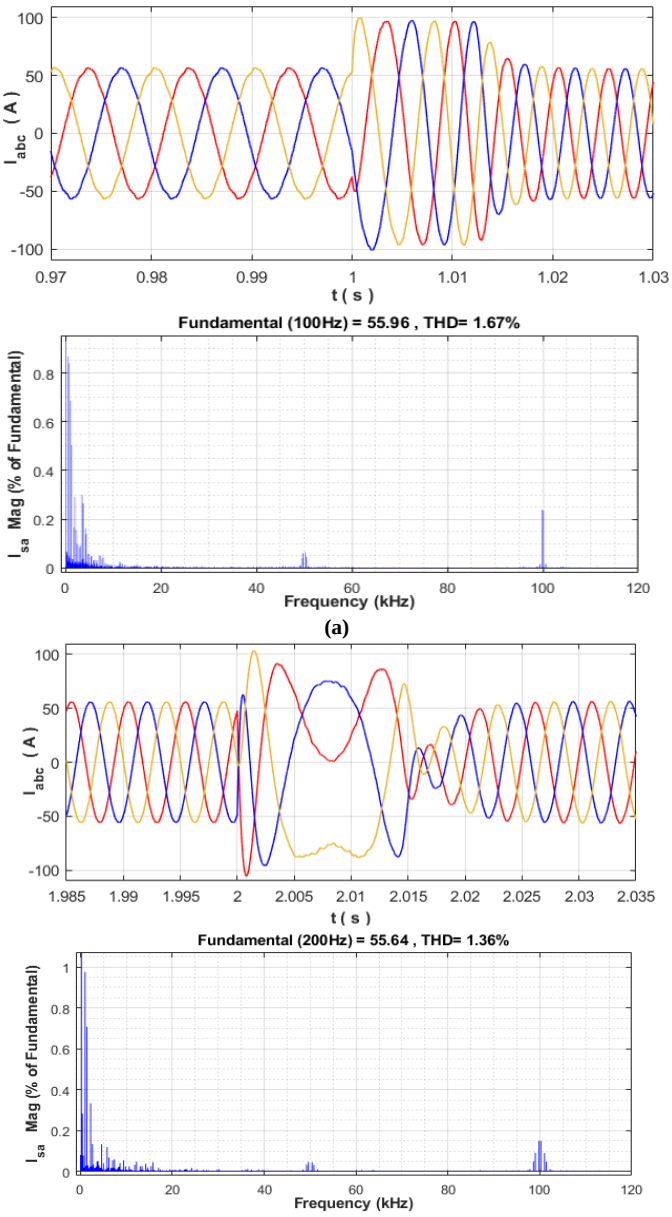

Fig.11. The stator currents for T_e= 40Nm, **a)** transition from +1500rpm to +3000rpm and THD analysis for t=0.5s, **b)**+3000rpm to -3000rpm and THD analysis for t=1.5s

The waveforms of the line-to-line voltages produced by the 3L T-Type inverter feeding the PMSM are given in Figure 12 (a) and (b). As seen from the figures, the inverter produces a three-level line-to-line voltage of 100 Hz for a speed of 1500rpm up to t =1s, while it produces a five-level voltage of 200Hz after reaching the reference speed of 3000 rpm. While it produces a three-level voltage of 100Hz during its transition to -3000 rpm reference speed at t=2s, it produces a five-level voltage of 200 Hz again when it reaches the reference speed. The harmonic analysis of the line-to-line voltage generated by the inverter while the PMSM is running at 3000rpm is given in Figure 13. As seen in the figure, the 3L T-Type inverter produces the fundamental harmonic has 269V amplitude and 200Hz frequency with a THD of 43.69%.

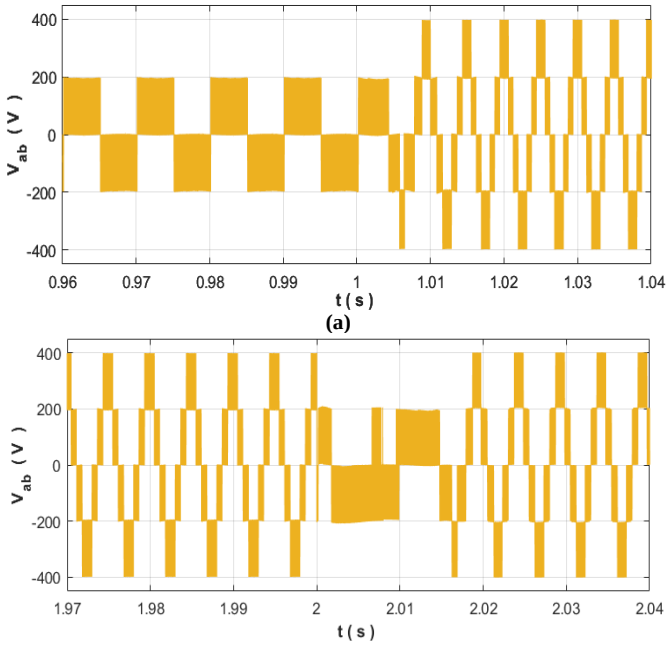

Fig.12. The line-to-line voltages of 3L T-Type inverter for transitions **a)** from 1500 to 3000 rpm, **b)** from 3000 to -3000 rpm

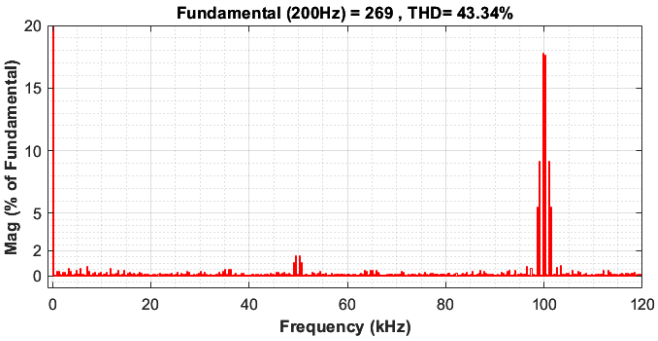

Fig.13. The THD analysis of line-to-line voltage (t=1.5 s)

The voltage change of the dc-link capacitors of the 3L T-Type inverter during the operation of the PMSM at different reference speeds is given in Figure 14. As seen in the figure, the voltage on each capacitor remained approximately constant at 200V, which is half of the dc voltage, in all operating states. While the fluctuations in capacitor voltages are a maximum of 10V during reference speed changes, it is seen that there is less fluctuation in steady states.

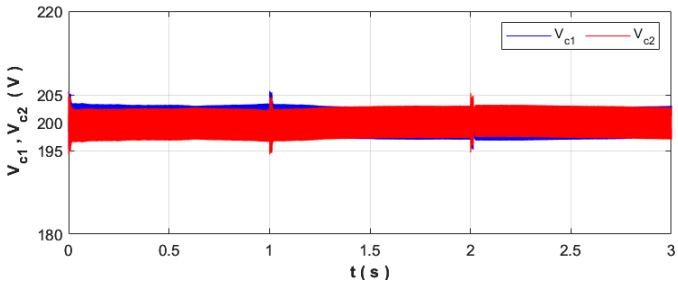

Fig.14. The dc-link capacitor voltages of T-type inverter

VI. Calculation of Power Losses for SiC MOSFET Based 3L T-type Inverter

The calculation of power losses for a power electronic converter is certainly done before starting the practical design. One of the most used methods is the calculation of semiconductor switches using datasheet information and any simulation program. The main purpose of these calculations is to obtain information about the efficiency of the entire system and to determine the size of the cooling system and fans to be used for the semiconductors in the application.

To calculate the efficiency of the 3L T-Type based 3-phase PMSM driver, it is necessary to calculate the inverter power losses. Nevertheless, gate drive losses are very small and often neglected. To calculate power losses, the current and voltage waveforms of all semiconductors and datasheet parameters such as turn-on resistance, turn-on and turn-off times, etc. are needed. In this study, the MSCSM120HRM163AG-SiC-MOSFET power module manufactured by Microchip for 3L T-Type applications is chosen for one phase leg of the inverter. The PCB layout's stray inductances will surely be reduced by using IPM modules rather than discrete MOSFETs. This module has four SiC MOSFETs, two (S_1-S_4) rated at 1200V, 138A (80°C), and two (S_2-S_3) rated at 700V, 98A (80°C). Body diodes (S_1, S_2, S_3, S_4) have similar values. While making this selection, the current value that the PMSM can draw in transient situations such as speed changes under full load is also taken into account.

In the simulation, the input power of the 3L T-Type inverter for 400V dc voltage is measured as P_{inp}=13.04kW, and the 3-phase ac output power of the inverter is measured as P_{out}=12.91kW as shown in Figure 15. In this case, the 3-phase T-type inverter has a power loss of about 1% (130W). However, to verify this power measurement, the power losses in the inverter circuit must also be calculated.

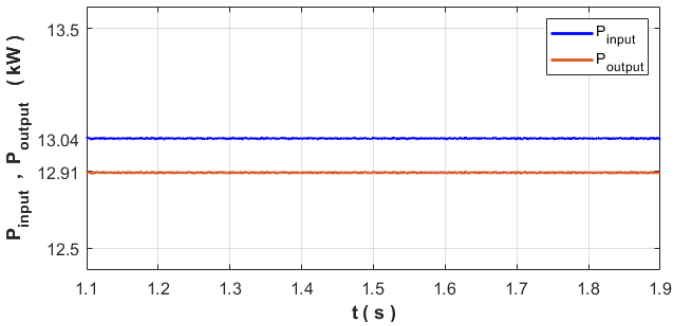

Fig.15. Input dc power and output 3-phase ac power of 3L T-type inverter

The IPM's datasheet parameters are used for the turn-on-resistance and voltage drop values of the MOSFETs and body diodes in the simulation. When the PMSM is operating at a 40Nm load and +3000rmp speed, the PWM signal, current and voltage waveforms for all semiconductors are measured for one period of voltage. As an example, the waveforms for S_{a1} and D_{a1} are given in Figure 16 (a) and for S_{a2} and D_{a2} in Figure 16 (b). To calculate the conduction and switching losses of each SiC MOSFET and conduction losses of body diodes, the average and rms values of MOSFET and body diodes current for both halves of the switching period are calculated separately

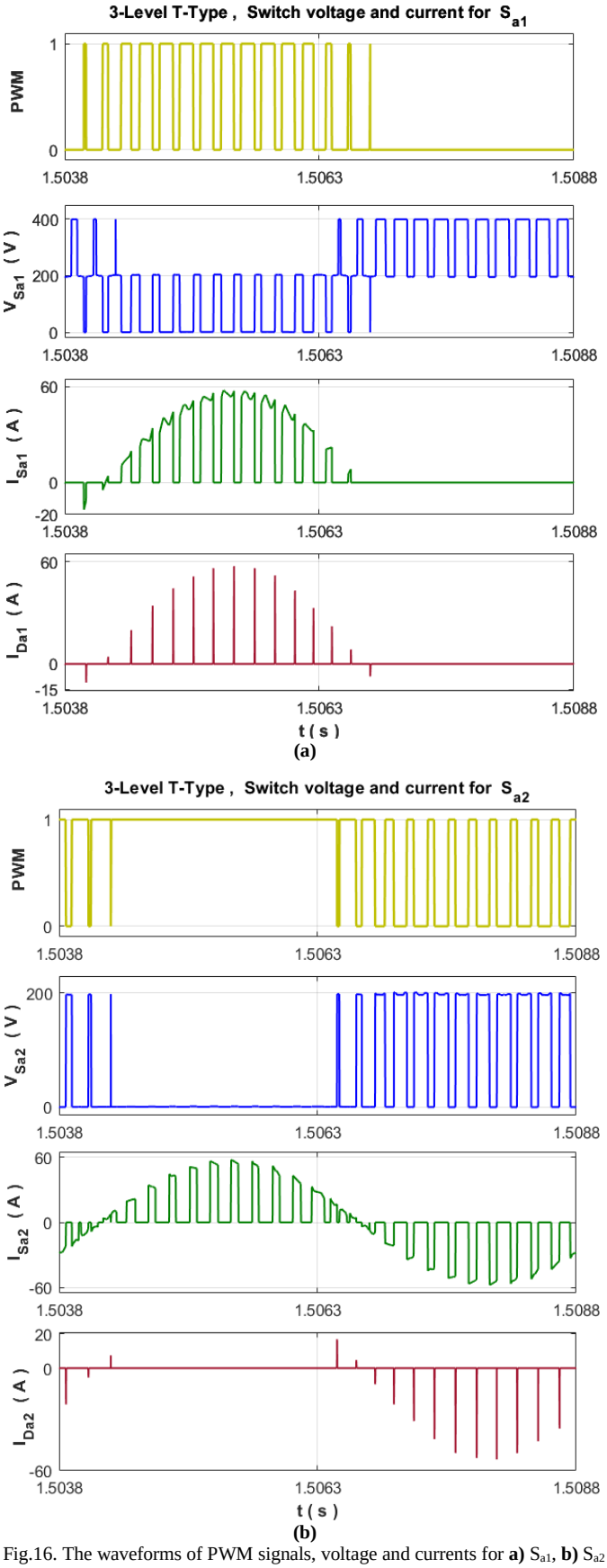

Fig.16. The waveforms of PWM signals, voltage and currents for **a)** S_{a1}, **b)** S_{a2}

TABLE III
I_{AVG} AND I_{RMS} VALUES FOR SiC MOSFET AND BODY DİODES

t	1.5038s – 1.5063s		1.5063s – 1.5088s	
	avg	rms	avg	rms
I_{Sa1}	21.62	31.50	0.027	1.41
I_{Sa2}	12.74	23.81	12.76	23.81
I_{Sa3}	12.72	23.76	12.76	23.81
I_{Sa4}	0.052	1.5	21.50	31.47
I_{Da1}	0.09	2.1	0.00023	0.16
I_{Da2}	0.0037	0.27	0.08	1.86
I_{Da3}	0.08	1.86	0.0037	0.27
I_{Da4}	0.002	0.22	0.092	2.10

in simulation and given in Table 3. These current values and datasheet parameters such as the MOSFETs' drain-source on resistance, turn-on delay time, rise time, turn-off delay time, and fall time values for 150°C junction temperature are substituted into Eq. (8)-(10) and the conduction and switching losses are calculated. This is because these values for SiC MOSFETs are the largest for a junction temperature of 150°C. This is also true for body diodes. Thus, for the most difficult operating conditions, such as large current and maximum junction temperature allowed in the datasheet, almost the largest possible power losses in the power circuit of the converter are calculated. In order to reduce the size of the passive components in the power circuit of the 3L T-Type inverter while not causing excessive EMI noise, the switching frequency is selected as 50kHz. Because overwhelming EMI noise makes the inverter hard to control and necessitates additional filters and an expensive PCB design. Conduction losses for the body diodes are also computed by substituting into Eq. (11) with the average current, rms current, voltage drop, and turn-on resistance values for a junction temperature of 150°C. The switching losses of the body diodes are neglected as they are very small. The total power loss in one period for 1-phase and 3-phase legs of T-Type is summarized in Table 4. The table shows that total losses calculated for 3-phase T-Type are about 1.0% for 50kHz. This result is compatible with the above measurement result. The bar representation of power losses in semiconductors is given in Figure 17. It is clearly seen that conduction losses are larger than switching losses in SiC MOSFETs. The body diode losses are quite small.

$$P_{Conduction\_S} = I_{rms}^2 \times R_{DS\,on}\,(T_j = 150\,^{\circ}C) \tag{8}$$

$$P_{on\_S} = \frac{1}{2} \times I_{DS} \times V_{DS} \times \frac{I_{DS}}{I_{DS\,Test}} \times \frac{V_{DS}}{V_{DS\,Test}} \times t_{on} \times f_s \tag{9}$$

$$P_{off\_S} = \frac{1}{2} \times I_{DS} \times V_{DS} \times \frac{I_{DS}}{I_{DS\,Test}} \times \frac{V_{DS}}{V_{DS\,Test}} \times t_{off} \times f_s \tag{10}$$

$$P_{Conduction\_Diode} = (I_{rms}^2 \times r_D) + (I_{avg} \times V_D) \tag{11}$$

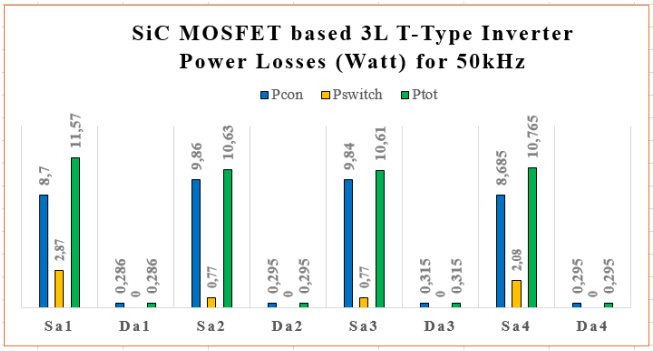

Fig.17. SiC MOSFET based 3L T-Type inverter power losses for 50kHz

TABLE IV
THE CONDUCTION AND SWITCHING LOSSES FOR 3L T-TYPE INVERTER WITH 50kHz

	1st Half Period			2nd Half Period			f_s=50kHz
	P_{Con}	P_{on}	P_{off}	P_{Con}	P_{on}	P_{off}	$P_{average}$
S_{a1}	17,36	1,84	2,3	0,034	0	0	21,53/2=10,767
D_{a1}	0,57	0	0	0,002	0	0	0,572/2=0,286
S_{a2}	9,86	0,41	0,36	9,86	0,41	0,36	21,26/2=10,63
D_{a2}	0,02	0	0	0,57	0	0	0,59/2=0,295
S_{a3}	9,82	0,41	0,36	9,86	0,41	0,36	21,22/2=10,61
D_{a3}	0,57	0	0	0,06	0	0	0,63/2=0,315
S_{a4}	0,04	0	0	17,33	1,85	2,31	21,53/2=10,765
D_{a4}	0,01	0	0	0,58	0	0	0,59/2=0,295
						Total losses for 1-leg of 3L T-Type	**42,772W**
						Total losses for 3-leg of 3L T-type	**128,32W**

$P_{out} = 13.040W - 128{,}32W = 12.911{,}68\,W$

$\eta\% = (12.911{,}68\,/13.040) \times 100 = 99\%$

VII. CONCLUSION

In this study, a compact and high-efficiency SiC MOSFET-based 3-level T-Type driver is proposed for PMSMs, which are widely used in many applications today. In this work, a SiC MOSFET based 3-level T-Type topology is proposed to build a compact and highly efficient dc/ac inverter that can be used in many low voltage (<1kV) applications. 3L T-Type already has a compact structure compared to other 3-level topologies. Also, due to a higher switching frequency operation, SiC-based T-Type inverter can become significantly more compact as they require much smaller passive elements and cooling arrangements. Since the Drain-Source on resistance of the preferred SiC MOSFETs is very small (17.5mΩ, 150C), the conduction losses of the 3L T-Type inverter are also small. The total power dissipation of the 3-phase 3L T-type inverter is calculated in detail for one period of the voltage for the worst case operation. The mathematically calculated power losses are approximately 1% and are in agreement with the measured power losses in the simulation. However, the power losses of all SiC MOSFETs are approximately equal, indicating that the power loss distribution is balanced.

APPENDIX A

Motor parameter values

Stator resistance R_a=0.0485Ω, d and q-axis inductance L_d= L_q=0.395mH, Moment of inertia J=0.0027$kg.m^2$, Friction coefficient B=0.0004924 $N.m.s$, Moment coefficient k_t=0.7164 N.m/A, Magnetic flux ϕ=0.1194$weber$, Electromagnetic moment T_e= 42.09Nm, Rated speed n_r=3000rpm, Number of pole pairs P=4, dc-link voltage V_{dc}=560V, Rotor Type = Round, Back emf= sinusoidal

ACKNOWLEDGMENT

The studies presented in this article were carried out within the scope of Berkan Turan's master thesis titled "Thesis Number:683667, Vector control of PMSM fed by three-phase three-level T-Type inverter, 2021". The advisor of the master's thesis is Assoc. Prof. Dr. Erkan Deniz

REFERENCES

[1] W. da S. Lima et al. "A bidirectional isolated integrated ac–dc converter based on an interleaved 3-level T-type power converters." IEEE Access, vol. 9, 2021, pp 142754-142767.

[2] R. Phukan et al. "Characterization and mitigation of conducted emissions in a SiC based three-level T-Type motor drive for aircraft propulsion." IEEE Transactions on Industry Applications, vol. 59.3, 2023, pp 3400-3412.

[3] E. Deniz, H. Altun. "Bes Seviyeli Izole DA Kaynakli Kaskat Inverterin SDGM Teknigi Ile Kontrolu." SAU Journal of Science, vol. 11. 1, 2007, pp 1–9.

[4] A. Nabae, I. Takahashi, H. Akagi. "A new neutral-point-clamped PWM inverter." IEEE Transaction Industrial Application, vol. IA. 17(5), 1981, pp 518–523.

[5] T. Bruckner, S. Bernet, H. Guldner. "The active NPC converter and its loss-balancing control." IEEE Transaction Ind. Electronics, vol. 52. 3, 2005, pp 855–868.

[6] M. Schweizer, I. Lizama, T. Friedli and J. W. Kolar, "Comparison of the chip area usage of 2-level and 3-level voltage source converter topologies." IECON 2010 - 36th Annual conference on IEEE Industrial Electronics Society. Glendale, AZ, 2010.

[7] Z. Wang, "Design and validation of a high-power, high density all silicon carbide three-level inverter." Ph.D Thesis, Electrical Engineering, University of Arkansas, 2021.

[8] Z. Wang, Y Wu, et al. "Busbar design and optimization for voltage overshoot mitigation of a silicon carbide high-power three-phase TNPC inverter." IEEE Transactions on Power Electronics, vol. 36.1, 2021, pp 204-214.

[9] A. I. Emon, Z. Yuan, A. B. Mirza, A. Deshpande, M. U. Hassan and F. Luo, "1200 V/650 V/160 A SiC+Si IGBT 3L Hybrid T-Type NPC Power Module With Enhanced EMI Shielding," in IEEE Transactions on Power Electronics, vol. 36, no. 12, 2021, pp 13660-13673.

[10] H. Peng, et al. "Improved space vector modulation for neutral-point balancing control in hybrid-switch-based TNPC neutral point-clamped inverters with loss and common-mode voltage reduction." CPSS Transactions on Power Electronics and Applications, vol. 4.4, 2019, pp 328-338.

[11] P. Azer, J. Bauman, "An asymmetric three-level T-type converter for switched reluctance motor drives in hybrid electric vehicles." 2019 IEEE Transportation Electrification Conference and Expo (ITEC), Detroit, MI, 2019.

[12] D. Xiao, J. Bauman, "Power loss comparison between three-level T-type and NPC converters with SVPWM and MPCC modulation schemes in electric vehicles." 2020 IEEE Transportation Electrification Conference and Expo (ITEC), Chicago, IL, 2020.

[13] R. A. Ghaderloo, C. Singhabahu, R. Resalayyan and A. Khaligh, "Selection of three-phase inverter topology and optimization of the pcb layout of a T-type bridge-leg for power dense motor drive application." 2024 4th International Conference on Smart Grid and Renewable Energy (SGRE), Doha, Qatar, 2024.

[14] Z. Yuan et al., "A 1.2 kV 400A SiC-Mosfet based 3L-TNPC power module with improved hybrid packaging method for high-density applications," 2021 IEEE Applied Power Electronics Conference and Exposition (APEC), Phoenix, AZ, USA, 2021.

[15] M. H. Adeli, E. Deniz, N. Altin, S. Ozdemir and A. Nasiri, "Compact GaN-Based 25kW, 480V Three-Level Active Front End Rectifier," 2024 IEEE Sixth International Conference on DC Microgrids (ICDCM), Columbia, SC, USA, 2024. doi: 10.1109/ICDCM60322.2024.10665131.

[16] A. Nasiri, M. H. Adeli, E. Deniz. "Active Neutral Point Clamped Electric Drive Converters Using WBG Devices." *Wide Bandgap Power Electronics, Emerging Converter Technologies and Applications*, edited by Isik C. Kizilyalli, Z. John Shen, Thomas M. Jahns, and Daniel W. Cunningham, Springer Cham, pp. 417-451, August, 2025. https://doi.org/10.1007/978-3-031-78631-0_16

[17] Z. Yuan et al., "A 1.2 kV 400A SiC-MOSFET Based 3L-TNPC Power Module with Improved Hybrid Packaging Method for High-Density Applications," 2021 IEEE Applied Power Electronics Conference and Exposition (APEC), Phoenix, AZ, USA, 2021.

[18] A. I. Emon et al, "1200 V/650 V/160 A SiC+Si IGBT 3L Hybrid T-Type NPC Power Module With Enhanced EMI Shielding," IEEE Transactions on Power Electronics, vol. 36.12, 2021, pp. 13660-13673.

[19] M. H. Adeli, N. Altin, E. Deniz, and A. Nasiri, "EMI Modeling of PCB-Based Three-Level Active Neutral-Point-Clamped GaN Converter." IEEE Applied Power Electronics Conference and Exposition (APEC2025), Atlanta, GA, USA, March 16-20, 2025. (Accepted).

[20] R. A. Ghaderloo, C. Singhabahu, R. Resalayyan and A. Khaligh, "Selection of Three-phase Inverter Topology and Optimization of the PCB Layout of a T-type Bridge-Leg for Power Dense Motor Drive Application," 2024 4th International Conference on Smart Grid and Renewable Energy (SGRE), Doha, Qatar, 2024.

[21] "PCB design techniques to reduces EMI", www.altium.com, 2024.

[22] "Conducted and Radiated Emissions Testing", Tektronix Application Note, pp 1-34

[23] R. Oberhuber. "Low-EMI designs for isolated ADC signal-chain solutions", Analog Design Journal, Texas Instrument, 2024.

[24] B. Turan, "Üç fazlı üç seviyeli T-Tipi inverterden beslenen sürekli mıknatıslı senkron motorun vektör kontrolü." Yüksek Lisan Tezi, Fırat Üniversitesi, Fen bilimleri Enstitüsü, Elektrik Elektronik Mühendisliği Teknolojileri Programı, 2021.

[25] C. Mohan, "A generalized predictive controlled TNPC power inverter with a deterministic dc-link capacitor voltage balancing approach." Master Thesis, Universidad De Sevilla Escuela Tecnica Superior De Ingenieria, Sevilla, 2015.

[26] E. Deniz, "ANN-based MPPT algorithm for standalone photovoltaic PMSM drive system without dc-dc boost converter." IENSC2018

International Engineering and Natural Sciences Conference, Diyarbakir, Turkiye, 14-17 November 2018.
[27] E. Deniz, "Medium and large vector-based SVPWM technique for five-phase two-level inverter." European Journal of Technique (EJT), vol.11.2, pp 209-216, 2021. https://doi.org/10.36222/ejt.1029249
[28] E. Deniz, O Aydogmus, "Comparison of asynchronous motor drives fed by three-level H-bridge inverter using SPWM and SVPWM. 6th International Advanced Technologies Symposium, Elazig/Turkey, pp. 448–454, May 16-18, 2011.
[29] B. Wu, *High-Power Converters and AC Drives*, IEEE Press, Hoboken, New Jersey, USA, 2006.
[30] A. Gündoğdu, "Matris konvertörden beslenen sabit mıknatıslı senkron motorun vektör kontrolünün sayısal benzetimi." Yüksek Lisans Tezi, Fırat Üniversitesi Fen Bilimleri Enstitüsü, 2005.
[31] Ö. Aydoğmuş, "Matris Çevirici ile beslenen sürekli mıknatıslı senkron motor sürücü tasarımı ve algılayıcısız hız denetimi." Doktora Tezi, Fırat Üniversitesi, Fen bilimleri Enstitüsü, 2011.
[32] A. Gundogdu, H. Altun, "Simulation of a RL load fed by a matrix converter with Matlab/Simulink." Journal of The Faculty of Engineering and Architecture of Gazi University, vol. 24.2), 2009, pp 199-207.
[33] A. Gundogdu, H. Kizmaz, R. Celikel, M. Yilmaz, "Speed sensorless adaptive power control for photovoltaic-fed water pump using extended Kalman–Bucy filter." Energy Reports, 10, 2023, pp. 1785–1795.

BIOGRAPHIES

Erkan Deniz was born in 1977. He received the B.S., M.S., and Ph.D. degrees from Firat University, Elazig, respectively in 2001, 2005, and 2011. From 2001 to 2012, he was a Research Assistant with the electrical teaching department. Since 2018, he has been an Associate Professor with the Electrical Electronics Engineering Department, Firat University. His research interests include power electronics, SiC MOSFETs, GaN FETs, pulse width modulation techniques, power quality, D-STATCOM, grid connected converters, energy storage systems, motor control, machine learning, CNN.

Berkan Turan was born in 1992. He received the B.S. from Gazi University, Ankara in 2014 and the M.S. from Fırat University, Elazığin 2021. He has been working as an electrical engineer at the Turkish State Railways since 2018. His research interests include grid connected converters, motor drivers.